

Highly active and robust Ni–MoS₂ supported on mesoporous carbon: A nanocatalyst for hydrodeoxygenation reactions

Swathi Mukundan,^{ab} Md A. Wahab,^c Luqman Atanda,^{ad} Muxina Konarova,^a and Jorge Beltramini^{*de}

^a *Nanomaterials center- AIBN and School of chemical engineering, The University of Queensland, Brisbane, QLD- 4072, Australia.*

^b *Department of applied chemistry, Cochin University of Science and Technology, Kochi, Kerala- 682022, India.*

^c *School of Chemistry, Physics and Mechanical Engineering, Faculty of Engineering, Queensland University of Technology, Brisbane, QLD- 4000, Australia.*

^d *Centre for Tropical Crops and Biocommodities, Queensland University of Technology, Brisbane, QLD- 4000, Australia.*

^e *IROAST, Department of Chemistry, Faculty of Advanced Science and Technology, Kumamoto University, Kumamoto 860-8555, Japan.*

Corresponding author E-mail: jorge.beltramini@qut.edu.au

Surface–structural properties and characteristics of carbon supports and supported NiMoS₂ catalysts

This study has considered two types of carbon supports: (i) microporous carbon – activated carbon (AC) which was used as received without modification (Fig. S1a and S1c) and (ii) mesoporous carbon – CMK–3 that was prepared *via* the mesoporous SBA–15 silica hard templating method (Fig. S1b and S1d). Fig. S1a shows the plate–like particles of AC whereas the morphology of CMK–3 shown in Fig. S1b exhibits a well–defined cylindrical rod–shaped particles.¹ Furthermore, the structural morphology of the pores obtained by TEM indicates AC is made of disordered irregular shaped pores (Fig. S1c), whereas CMK–3 has an organized mesoporous structure along with excellent pore connectivity (Fig. S1d).

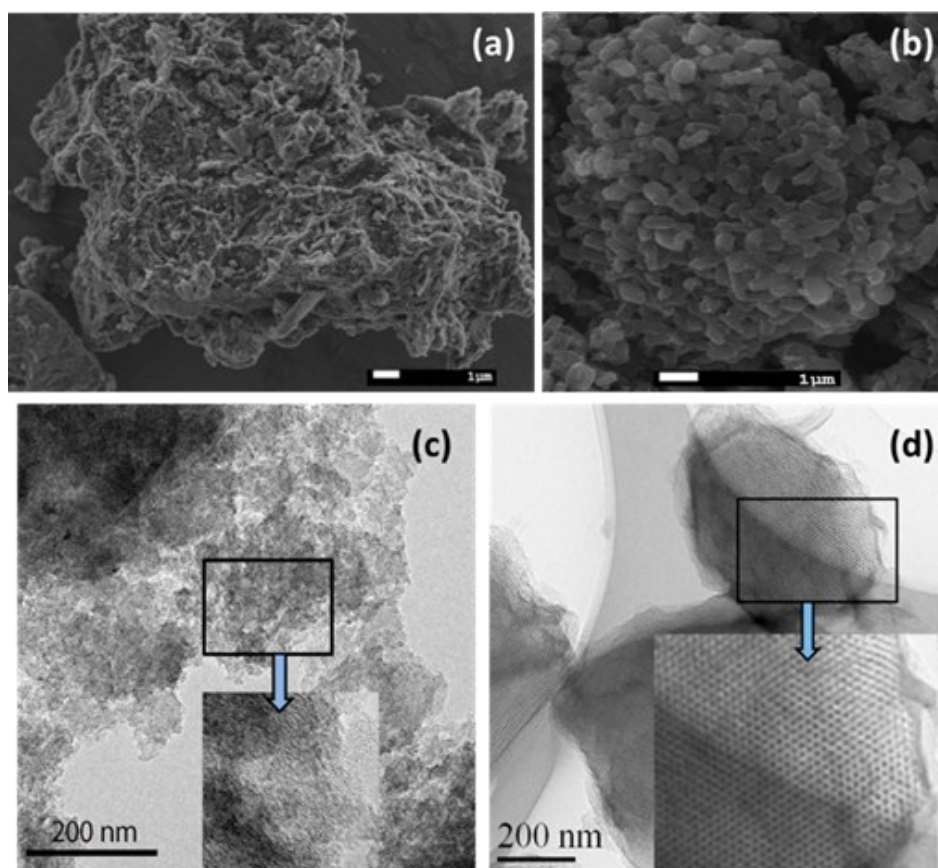


Fig. S1 SEM and TEM images of AC (a and c) and CMK–3 (b and d) supports

The nitrogen adsorption–desorption isotherm of CMK–3, shown in Fig. S2, is typical of a type IV isotherm with H2 hysteresis loop and an average PSD of 3.85 nm that is characteristic of mesoporous materials and results of which are consisted with previous reports on mesoporous CMK–3 and also with IUPAC classification made for type IV for mesoporous structures, could be supported by the TEM image in Figure 1d.²⁻⁷ On the other hand, AC displays an isotherm typical of microporous materials with H4 hysteresis loop with a broad range of PSD that shows an average mesopore size of 3.85 (34 %) along with predominant micropores (66 %) in the range of 0.4 to 2 nm seen at a relatively low pressure consisted with previously published works on AC type materials.^{8, 9} Fig. S2 shows the nitrogen adsorption–desorption isotherms of the various studied carbon supports (AC, CMK–3) and the supported catalysts (MoS₂/AC, MoS₂/CMK–3, NiMoS₂/AC, NiMoS₂/CMK–3) and their corresponding and BJH– pore size distribution (PSD) curves are also shown in the inset of Fig. S2.

Table S1 BET surface area and pore volume of AC, CMK–3 supports along with the supported catalysts (MoS₂/AC, MoS₂/CMK–3, NiMoS₂/AC and NiMoS₂/CMK–3)

Support/catalyst	BET Surface area (m ² g ⁻¹)		Pore Volume (cm ³ g ⁻¹)			Pore Size (nm) ^b
	Micro ^a	Total	Micro	Meso	Total	
AC	705	1063	0.36	0.62	0.98	3.85
CMK–3	96	1258	0.05	1.19	1.24	3.85
MoS ₂ /AC	49	165	0.003	0.27	0.27	3.8
NiMoS ₂ /AC	45	153	0.023	0.19	0.21	3.7
MoS ₂ /CMK–3	23	562	0.008	0.84	0.85	3.5
NiMoS ₂ /CMK–3	0	453	0	0.33	0.33	3.6

^aCalculated from BET t–Plot micropore area, ^bpore size calculated by BJH method from desorption isotherm.

All the supported metal nanocatalysts followed a similar trend of the N₂ adsorption–desorption isotherm as the parent support, which is consistent with the previous reports on the functionalized and or metal functionalized mesoporous structures.¹⁰ For instance, AC support has a BET surface area of 1063 m²/g and a total pore volume of 0.98 cm³/g (Table S1). Upon the deposition of MoS₂, surface area decreased to 165 m²/g (i.e. 84.47% reduction) which declines further to 153 m²/g (i.e. another 7.27 % reduction) after the incorporation of Ni. The pattern of surface area reduction is an indication that the predominantly available micropores of AC were blocked by the deposition of MoS₂ species. On the other hand, the total reduction of surface area of NiMoS₂/CMK–3 was found to be reduced by 19.4 % after the incorporation of Ni into MoS₂/CMK–3 (453 m² g⁻¹ from 562 m² g⁻¹ for MoS₂/CMK–3). Furthermore, the pore volume was found to have decreased from 0.85 (MoS₂/CMK–3) to 0.33 (NiMoS₂/CMK–3). It is found that the pore size distribution of the MoS₂/CMK–3 support was not changed after the incorporation of Ni into MoS₂/CMK–3. Therefore, this reduction in surface area and particularly reduction in mesopore volume (61.17 % reduction from 0.85 cm³/g for MoS₂/CMK–3) in Table S1 would not be the case if the Ni species were not preferentially incorporated inside the mesopores of this support. These results are consistent with the previous reports on the formation/incorporation of active species within the pores of the porous structure.¹¹ From this result, we can infer that CMK–3 has a superior surface–structural properties that benefited the incorporation and dispersion of metal/active species, which could significantly impact catalytic property of the materials.

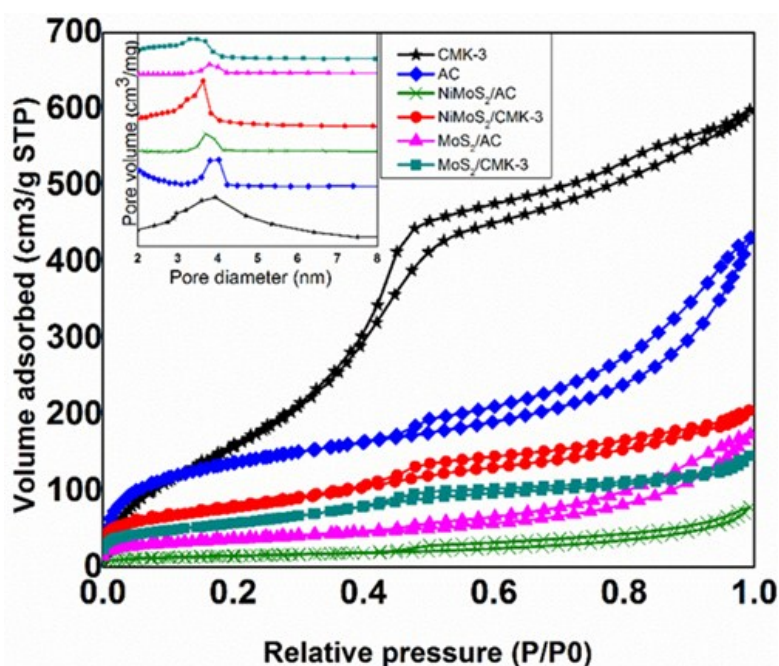


Fig. SS2 F N₂ adsorption–desorption isotherms and pore size distribution curves (inset) of AC, CMK–3, MoS₂/AC, MoS₂/CMK–3, NiMoS₂/AC and NiMoS₂/CMK–3.

The small-angle XRD patterns of CMK-3 (Fig. S3a) exhibit the presence of three well-resolved reflections (100), (110), and (200) at 0.9° , 1.6° and 1.8° respectively, corresponding to the formation of hexagonal mesoporous carbon structure.¹² However, after incorporating the metal species onto the CMK-3 support the intensity of these peaks was greatly reduced in both $\text{MoS}_2/\text{CMK-3}$ and $\text{NiMoS}_2/\text{CMK-3}$. According to previous reports,¹⁰ the attenuation of the XRD peaks for metal species functionalized CMK-3 is due to the X-ray scattering contrast between the mesoporous framework walls and functional moieties that are inside the mesoporous nanochannels, indicating the incorporation of metal species onto the CMK-3 support, which is also very consistent with the reduced surface-structural properties in Table S1 for the metal incorporated CMK-3/AC materials. The higher angle XRD patterns of CMK-3 and AC supports (Fig. S3b) display the presence of the graphitic nature of carbon framework but the peak intensity of CMK-3 is greater than that of AC, suggesting the better graphitic nature of CMK-3. From Fig. S3b, also the peaks at $2\theta = 39.1^\circ$ and 69.8° found in all the supported catalysts correspond to MoS_2 species in the carbon framework whereas the other peaks at $2\theta = 25.5^\circ$, 36.4° , 58.8° and 64.6° could be ascribed to (111), (311), (511) and (440) planes of Ni_3S_4 that matched well with the values found in the literature.¹³

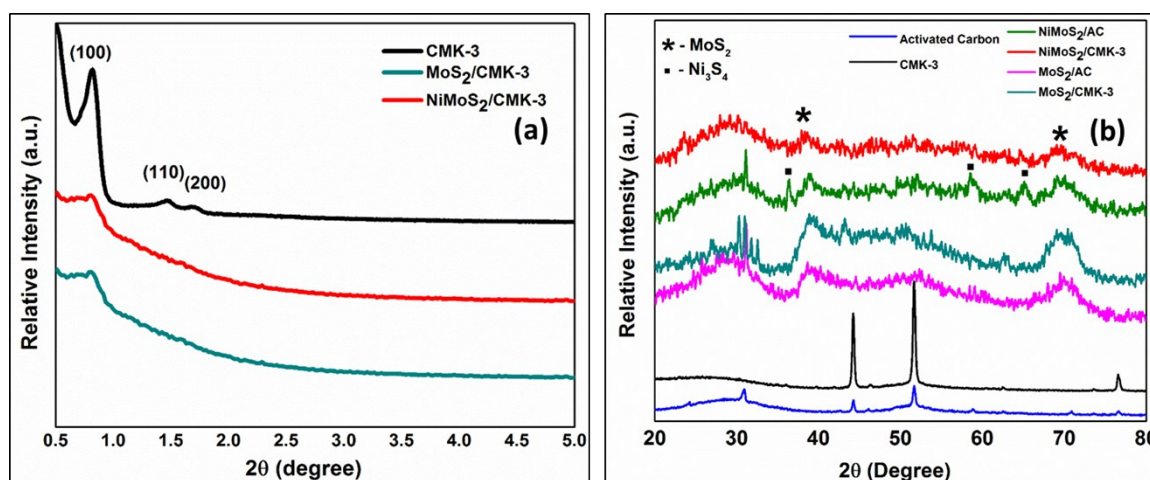


Fig. S3 (a) Small angle XRD of CMK-3, $\text{MoS}_2/\text{CMK-3}$, $\text{NiMoS}_2/\text{CMK-3}$ and (b) Wide angle XRD patterns of (1) AC, (2) CMK-3, (3) MoS_2/AC , (4) $\text{MoS}_2/\text{CMK-3}$, (5) NiMoS_2/AC and (6) $\text{NiMoS}_2/\text{CMK-3}$.

The Raman spectra of AC and CMK-3 supports in Fig. S4 exhibited two sharp peaks at 1340 and 1600 cm^{-1} which could be assigned to the D band and G bands, respectively, that arises from the disordered and graphitic structure of carbon framework.¹⁴ The ratio of the difference in intensities between D and G bands (I_D/I_G) gives the extent of graphitization in the carbon framework. The calculated I_D/I_G ratio values for the studied samples were found to be 0.98 and 0.89 for AC and CMK-3, respectively and the results shows the high defectiveness of AC. The Raman spectra of supported catalysts in the inset of Fig. S4 displayed bands at 405 cm^{-1} and 382 cm^{-1} which are characteristics of E_{2g}^1 and A_{1g} Raman vibrations, respectively, which correspond to S-Mo-S bonding in MoS_2 species, suggesting the incorporation of metal species in the final carbon supports.¹⁵

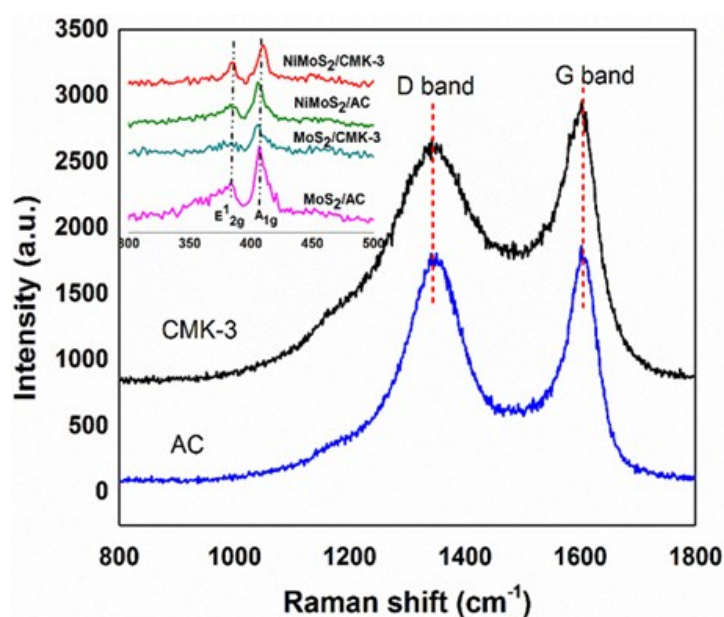


Fig. S4 Raman spectra of AC and CMK-3 supports, MoS_2/AC , $\text{MoS}_2/\text{CMK-3}$, NiMoS_2/AC and $\text{NiMoS}_2/\text{CMK-3}$ (inset).

The XPS wide scan survey spectra of the samples in Fig. S5 reveals that the supports consist of mainly carbon with minor oxygen content. The wide scan survey spectra also confirms the presence of Mo, S and Ni for the supported catalysts. From the peak deconvolution of the C1s regions for CMK-3 and AC supports shown in Fig. S6(a) and (b), respectively, we observed a major peak at 284.6 eV ascribed to the presence of C (sp²) and C-C (sp³) bonding of graphitic structure which was used as a reference for calibration purpose.¹⁶ The peaks associated with pi-pi satellite, C-O-C and O-C=C are outlined in the graphs as well.¹⁷ The O1s spectrum of carbon support in Fig. S6(c) and (d) exhibits peaks corresponding to C-O and C-O-H at 531.9 eV and 533.3 eV, respectively. Moreover, minor peaks at 530.4 eV and 536.6 eV corresponding to Si-O and Na Auger, respectively, were also observed on AC.¹⁸ These results are well-consistent with previous reports on the mesoporous carbon and activated carbon materials.¹⁹

The curve-fitted XPS spectra of Mo 3d, S 2p and Ni 2p regions are also illustrated in Fig. S6 (e) to (j). Both NiMoS₂/AC and NiMoS₂/CMK-3 catalysts exhibited similar Mo oxidation states, Mo⁺⁴ and Mo⁺⁶. Binding energies observed at 229.5 eV and 232.6 eV represents the Mo 3d_{5/2} and Mo 3d_{3/2} spin orbits of Mo⁺⁴, respectively, whereas the 233.1 eV and 236.2 eV represent Mo 3d_{5/2} and Mo 3d_{3/2} of Mo⁺⁶, respectively (Fig. S6 (e) and (f)). The presence of a peak at 226.8 eV shows the S 2s bond to Mo. The formation of Ni₃S₄ phase can also be seen in both NiMoS₂/AC and NiMoS₂/CMK-3 catalysts. Ni₃S₄ and Ni²⁺ species exhibit binding energy values of 854.1 eV and 856.9 eV that correspond to Ni₃S₄ and Ni²⁺ species, respectively, which can be seen in Fig. S6 (g) and (h).

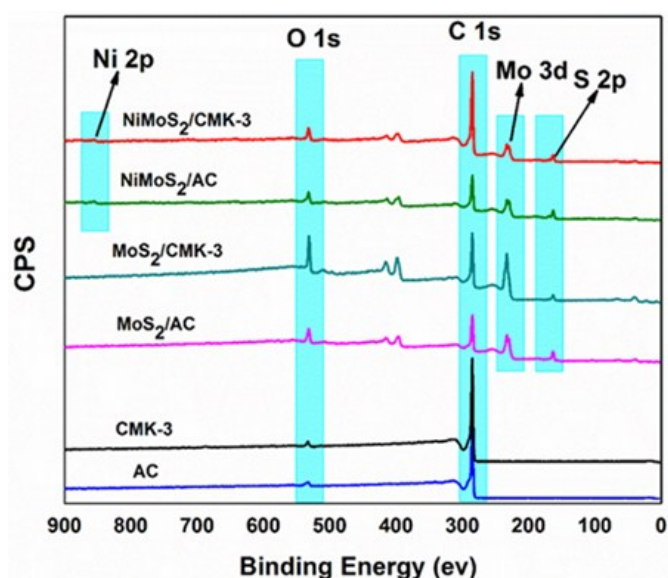


Fig. S5 The XPS wide scan survey spectra carbon supports and supported catalysts.

Table S2 Surface and bulk elemental composition (at. %) of MoS₂/AC, MoS₂/CMK-3, NiMoS₂/AC and NiMoS₂/CMK-3 catalysts

Catalyst	Surface elemental composition ^a (at. %)					Bulk elemental composition ^b (at. %)				
	Ni	Mo	S	S/Mo	Ni/Mo	Ni	Mo	S	S/Mo	Ni/Mo
MoS ₂ /AC	–	5.3	10.3	1.95	–	–	1.9	3.92	2.06	–
MoS ₂ /CMK-3	–	5.0	9.9	1.98	–	–	1.82	3.66	2.01	–
NiMoS ₂ /AC	1.52	4.9	9.3	1.90	0.31	0.44	1.76	3.43	1.95	0.25
NiMoS ₂ /CMK-3	0.76	4.75	9.1	1.92	0.16	0.43	1.70	3.36	1.98	0.25

^aAnalysed by XPS, catalysts are reduced before analysis but not protected from exposure to air. ^bAnalysed by ICP, catalysts are reduced before analysis but not protected from exposure to air.

Sulphur is present in the catalyst as both sulphide and sulphate. The formation of sulphate was due to the presence of atmospheric oxygen during synthesis and also from the carbon supports as XPS has shown oxygen peaks.

The binding energy values of 162.3 eV and 163.5 eV indicate the S 2p_{3/2} and S 2p_{1/2} of sulphide compounds, respectively. The peak at 169.8 eV is associated with the sulphate in Fig. S6 (i) and Fig. S(j).

The bulk elemental compositions of the supported catalysts were analysed by ICP and their corresponding values (at. %) are given in Table S2 were compared to the surface analysis from XPS. For all the catalysts, the S to Mo atomic ratio was around 2:1, the same for both the bulk and surface analysis, –showing that Mo is in the sulphided state. In terms of the distribution of Ni species in the NiMoS₂/AC catalyst, the bulk composition has a Ni/Mo ratio of 0.25, while the Ni/Mo ratio was 0.32 at the surface, suggesting the presence of higher concentration of Ni species on the surface of the catalyst. Similarly in the case of NiMoS₂/CMK-3, the bulk composition of both Ni and Mo species gave a Ni/Mo ratio of 0.25 but the surface concentration was as low as 0.16% Ni per Mo atom, which was almost half as the distribution found with the AC supported catalyst. This clearly indicates that the Ni species get deposited predominantly inside the pores of the CMK-3 supported catalysts whereas the MoS₂ fringes are present outside the pores. This hypothesis is validated by the drastic decrease in the pore volume of CMK-3 after the deposition of Ni species as measured by BET (Table S1). This kind of drastic reduction of pore volume could only happen if active species migrates into the pores otherwise active species loosely bound outside of the surface will be leached out during the course of reactions.

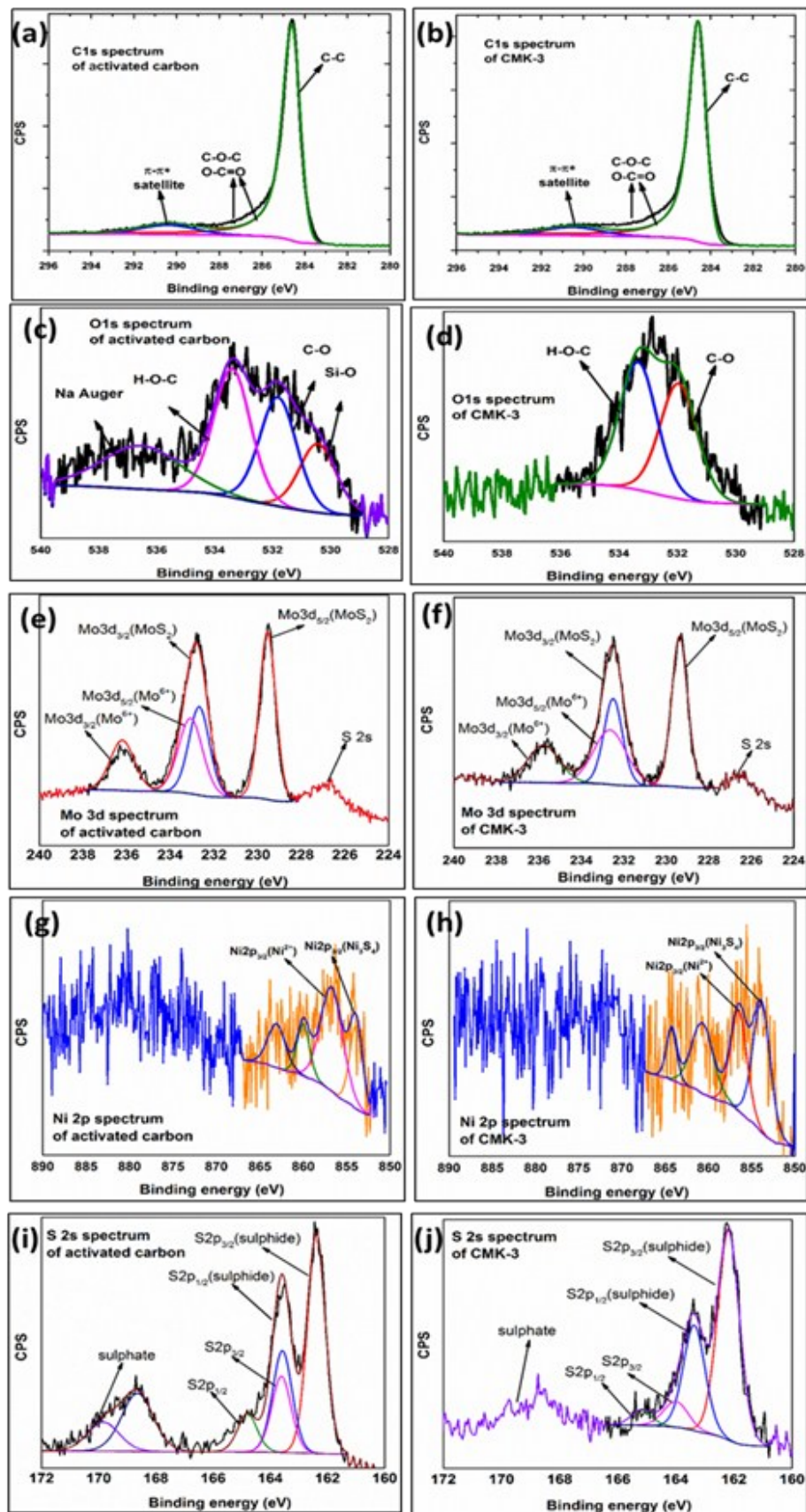


Fig. S6 C 1s, O 1s, Mo 3d, Ni 2p and S 2s XPS spectra of NiMoS₂/AC and NiMoS₂/CMK-3 supports.

References

1. K. S. W. Sing, D. H. Everett, R. A. W. Haul, L. Moscou, R. A. Pierotti, J. Rouquerol and T. Siemieniewska, in *Handbook of Heterogeneous Catalysis*, Wiley-VCH Verlag GmbH & Co. KGaA, 2008, DOI: 10.1002/9783527610044.hetcat0065.
2. L. Rivoira, J. Juárez, H. Falcón, M. G. Costa, O. Anunziata and A. Beltramone, *Catalysis Today*, 2017, **282**, 123-132.
3. S. Jun, S. H. Joo, R. Ryoo, M. Kruk, M. Jaroniec, Z. Liu, T. Ohsuna and O. Terasaki, *Journal of the American Chemical Society*, 2000, **122**, 10712-10713.
4. X. Ji, K. T. Lee and L. F. Nazar, *Nature Materials*, 2009, **8**, 500.
5. E. P. Barrett, L. G. Joyner and P. P. Halenda, *Journal of the American Chemical Society*, 1951, **73**, 373-380.
6. M. A. Wahab, Y. Jia, D. Yang, H. Zhao and X. Yao, *Journal of Materials Chemistry A*, 2013, **1**, 3471-3478.
7. M. A. Wahab, D. J. Young, A. Karim, S. Fawzia and J. N. Beltramini, *International Journal of Hydrogen Energy*, 2016, **41**, 20573-20582.
8. C. Fan, V. Nguyen, Y. Zeng, P. Phadungbut, T. Horikawa, D. Do and D. Nicholson, *Microporous and Mesoporous Materials*, 2015, **209**, 79-89.
9. C. G. Burgess, D. H. Everett and S. Nuttall, *Pure and Applied chemistry*, 1989, **61**, 1845-1852.
10. L. Li, Z. H. Zhu, G. Q. Lu, Z. F. Yan and S. Z. Qiao, *Carbon*, 2007, **45**, 11-20.
11. M. Ferrari, B. Delmon and P. Grange, *Microporous and Mesoporous Materials*, 2002, **56**, 279-290.
12. B. Kuppam and P. Selvam, *Progress in Natural Science: Materials International*, 2012, **22**, 616-623.
13. L. Wang, J. Liu, L. L. Zhang, B. Dai, M. Xu, M. Ji, X. S. Zhao, C. Cao, J. Zhang and H. Zhu, *RSC Advances*, 2015, **5**, 8422-8426.
14. F. Su, J. Zeng, X. Bao, Y. Yu, J. Y. Lee and X. S. Zhao, *Chemistry of Materials*, 2005, **17**, 3960-3967.
15. A. G. Bagnall, W. Y. Liang, E. A. Marseglia and B. Welber, *Physica B+C*, 1980, **99**, 343-346.
16. J. L. Pinilla, H. Purón, D. Torres, I. Suelves and M. Millan, *Carbon*, 2015, **81**, 574-586.
17. H. Kobayashi, H. Kaiki, A. Shrotri, K. Techikawara and A. Fukuoka, *Chemical Science*, 2016, **7**, 692-696.
18. J. F. Moulder, *Physical electronics*, 1995, 230-232.
19. D. Lennon, D. Lundie, S. Jackson, G. Kelly and S. Parker, *Langmuir*, 2002, **18**, 4667-4673.